




OCTOBER 08 2024

Deep sediment heterogeneity inferred using very low-frequency features from merchant ships^{a)}

Alexandra M. Hopps-McDaniel ; Tracianne B. Neilsen ; D. P. Knobles; William S. Hodgkiss; Preston S. Wilson ; Jason D. Sagers

 Check for updates

J. Acoust. Soc. Am. 156, 2265–2274 (2024)

<https://doi.org/10.1121/10.0030467>



View Online



Export Citation

Articles You May Be Interested In

Influence of seabed on very low frequency sound recorded during passage of merchant ships on the New England shelf

J. Acoust. Soc. Am. (May 2021)

Seabed classification from merchant ship-radiated noise using a physics-based ensemble of deep learning algorithms

J. Acoust. Soc. Am. (August 2021)

Source level predictions of surface ships using seabed characterization in the New England Mudpatch from viscous grain shearing model




J. Acoust. Soc. Am. (October 2019)



LEARN MORE

Advance your science and career as a member of the
Acoustical Society of America

Deep sediment heterogeneity inferred using very low-frequency features from merchant ships^{a)}

Alexandra M. Hopps-McDaniel,^{1,b)}  Tracianne B. Neilsen,^{1,c)}  D. P. Knobles,² William S. Hodgkiss,³ Preston S. Wilson,^{4,5}  and Jason D. Sagers⁵

¹Department of Physics and Astronomy, Brigham Young University, Provo, Utah 84602, USA

²The Platt Institute, P.O. Box 27200, Austin, Texas 78755, USA

³Marine Physical Laboratory, Scripps Institution of Oceanography, University of California, San Diego, La Jolla, California 92093, USA

⁴Walker Department of Mechanical Engineering, University of Texas at Austin, Austin, Texas 78712-1591, USA

⁵Applied Research Laboratories, The University of Texas at Austin, Austin, Texas 78766-9767, USA

ABSTRACT:

The very low-frequency noise from merchant ships provides a good broadband sound source to study the deep layers of the seabed. The nested striations that characterize ship time-frequency spectrograms contain unique acoustic features corresponding to where the waveguide invariant β becomes infinite. In this dataset, these features occur at frequencies between 20 and 80 Hz, where pairs of modal group velocities become equal. The goal of this study is to identify these $\beta = \infty$ frequencies in ship noise spectrograms and use them to perform statistical inference for the deep layer sound speeds and thicknesses in the New England Mudpatch for a larger number of ships and acoustic arrays over a larger geographical region than previously studied. Marginal probability distributions of the data indicate that using singular points for a feature-based inversion yields an estimate of the sound speed and a limiting value for the thickness of the first deep layer. Heterogeneity is examined by correlating spatial variability of the deep layer sound speeds with ship tracks. © 2024 Acoustical Society of America. <https://doi.org/10.1121/10.0030467>

(Received 12 June 2024; revised 16 August 2024; accepted 20 September 2024; published online 8 October 2024)

[Editor: James F. Lynch]

Pages: 2265–2274

I. INTRODUCTION

Sediment characterization studies often focus on the upper portions of seabed.^{1–8} However, sub-bottom profiling usually indicates the presence of deep layers.^{9,10} While large seismic studies with, for example, air gun sources and long arrays can infer information about the deep layering of the seabed, the inference of the deep layer structure from ambient noise can play a complementary role.

Results from the Seabed Characterization Experiment (SBCEX) 2017, which took place in the New England Mud Patch (NEMP), indicated heterogeneity in the thickness of the top layers of the seabed. However, less work has been done to study the sediment structure deeper than 18 m. An overview paper by Wilson *et al.*¹¹ provides a synthesis of some of the results obtained from SBCEX 2017 measurements, including seabed coring, direct measurements, and short- and long-range remote sensing. The general consensus is that the top layer of the NEMP seabed consists of a fine-grained sediment with variable thickness between about 5 and 12 m. The location of SBCEX 2017 is close to the area of a large seismic study that took place in 2009 by Siegel *et al.*,¹² which provided a measure of ground truth for

deeper sediment layers in the seafloor between the mud base and the basement.

The goal of this paper is to take advantage of the broadband noise sources provided by passing merchant ships to infer characteristics of the deeper layers of the NEMP. This study uses similar methods to those reported by Knobles *et al.*^{13,14} We expand the previous SBCEX 2017 study by using a larger sample of merchant ship noise recorded on three acoustic arrays during SBCEX 2022. The results from this analysis indicate heterogeneity of the seabed in the deep layers of the NEMP.

The rest of this paper is organized as follows. Section II provides a description of merchant ship tracks in the NEMP, acoustic arrays, and methods used to infer knowledge from the ship spectrograms. Section III provides the results of a statistical inference technique to estimate the deep layer sound speeds in the NEMP. Section IV draws conclusions from the sound speed results regarding deep layer heterogeneity.

II. METHODOLOGY

A. SBCEX

The SBCEX was a multiyear multi-institutional project to characterize the seabed of the NEMP, which is south of Martha's Vineyard, MA. As discussed in Wilson *et al.*,¹¹ the main goal of the project was to understand the physical

^{a)}This paper is part of a special issue on Assessing Sediment Heterogeneity on Continental Shelves and Slopes.

^{b)}Email: mcdaniel.alexh@gmail.com

^{c)}Email: tbn@byu.edu

mechanisms that control acoustic propagation in fine-grained sediments. Their paper also provided an overview of additional goals and motivation of analyses as well as a summary of the acoustic sources and arrays used during the experiments conducted in March of 2017. The goals, acoustic sources, and acoustic arrays used in the SBCEX 2022 were similar to those of SBCEX 2017, with one major change being the month, which led to greater variation in the water column. This change was a result of SBCEX 2022 being two months later in the year than the 2017 experiment. In March 2017, the seasonal storms caused the waters to be well-mixed; in May 2022, a depth-dependent temperature profile was established. In particular, the increase in the sound speed in the lower portion of the water column was caused by the intrusion of warmer, saltier waters from the southern hemisphere carried by the Gulf Stream.^{15,16} A comparison of the sound speed profiles from SBCEX 2017 and 2022 is shown in Fig. 1. The focus of the analyses in this work is merchant ship noise recorded during SBCEX 2022.

During SBCEX 2022, three vertical line arrays (VLAs) were deployed strategically between two shipping lanes. The average water depth in the geographical area is 75 m. Two of the arrays from Marine Physical Laboratory, Scripps Institution of Oceanography (MPL), referred to as VLA1 and -2, were placed approximately 6.7 km apart (with about 1 m bathymetry difference between them) and were deployed at this location for three days. The third array, from Applied Research Laboratories, The University of Texas at Austin (ARL), referred to as PROTEUS, was deployed for 28 days located between VLA1 and -2. All three arrays were deployed at the same locations as in SBCEX 2017. The coordinates and deployment dates are shown in Table I.

B. $\beta \rightarrow \infty$ singular points

The waveguide invariant β is a scalar quantity used to describe dispersive propagation characteristics in an ocean environment and is related to the slope of a striation in

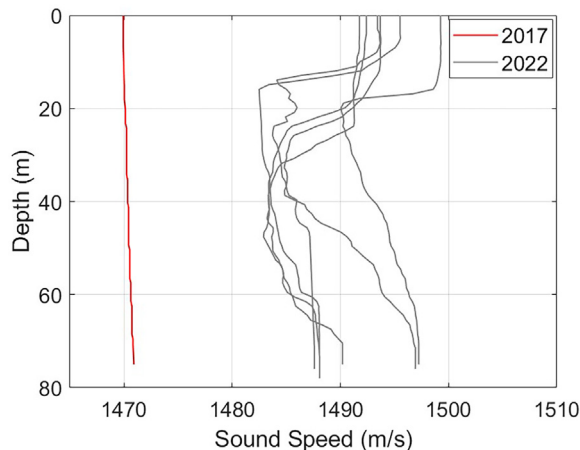


FIG. 1. (Color online) Examples of measured sound speed profiles from SBCEX 2017 and 2022.

range-frequency space.¹⁷ First proposed by Chuprov,¹⁸ β was developed as an alternative to range localization via matched-field processing.¹⁹ It has also been used for waveguide parameter estimation.^{20,21} Other studies, such as the one done by Verlinden *et al.*,²² have used ship spectrograms to estimate the waveguide invariant throughout a geographical area.

The waveguide invariant is related to the slope of the striations in range-frequency space,

$$\frac{\partial r}{\partial \omega} = -\frac{r}{\omega} \beta_{m,n}(\omega). \quad (1)$$

The $\beta_{m,n}(\omega)$ can also be expressed as a function independent of range r and only related to the frequency and modal properties using normal mode theory²³ [e.g., in the derivation in Eqs. (1)–(18) of Knobles *et al.*¹³] In this formulation, $\beta_{m,n}(\omega)$ is the difference in the inverse modal phase velocity, $C(\omega)$, over the difference in the inverse modal group velocity, $V(\omega)$, between modes m and n for frequency $f = \omega/2\pi$:

$$\beta_{m,n}(\omega) = \frac{\frac{1}{C_m(\omega)} - \frac{1}{C_n(\omega)}}{\frac{1}{V_m(\omega)} - \frac{1}{V_n(\omega)}}. \quad (2)$$

As seen in Eq. (2), the value for $\beta_{m,n}(\omega)$ goes to infinity at frequencies where the group velocities of modes m and n are equal. This $\beta \rightarrow \infty$ condition results in a particular feature in ship spectrograms: an “X” pattern where the nested striations switch directions and the acoustic intensity of striations of time-frequency spectrograms possess discontinuities.

Knobles *et al.*^{13,14} first observed these acoustic features, referred to as singular points, in the very low-frequency (VLF) bands of merchant ships in the NEMP during SBCEX 2017. The discrete spectrum of the $\beta = \infty$ frequencies for low mode numbers allows for the inference of seabed parameters of deep layers in the seafloor. Because $\beta_{m,n}$ is a modal parameter, it depends only on the environment. The singular frequencies ($f_{m,n}$) at which $\beta_{m,n} \rightarrow \infty$ are independent of source-receiver range and source-receiver depth, as well as the ship speed and size. Using singular points from five ships traveling through the southern shipping lane recorded on a single array, the previous SBCEX 2017 waveguide invariant study was able to estimate the deep layer sound speeds and a lower limit of the sediment thicknesses in the NEMP.

TABLE I. Coordinates and deployment dates of the VLAs.

VLA	Latitude	Longitude	Date of:	
			Deployment	Retrieval
VLA1	40.4700	-70.5971	23 May 2022	26 May 2022
PROTEUS	40.4590	-70.5635	7 May 2022	3 June 2022
VLA2	40.4418	-70.5272	23 May 2022	26 May 2022

A few other recent studies have investigated deep layer properties. Piao *et al.*²⁴ analyzed data taken in the Yellow Sea, where a 4.1 km 336-channel horizontal array was towed behind a ship with an air gun acoustic source. In addition to the standard array processing for seabed layering information, they took advantage of the observed singularities where $\beta_{m,n} \rightarrow \infty$ frequencies to estimate deep layer sound speeds, layer thickness, and a basement sound speed. Another study by Koch and Knobles²⁵ took advantage of the low-frequency features of broadband noise that merchant ships provide when passing close to acoustic receivers to ascertain deep layer structures.

C. Merchant ships

Time-frequency spectrograms of the received acoustic intensity of ships are characterized by a nested hyperbola pattern, often referred to as *striations*. For the present study, the spectrogram time interval is selected to be centered at the closest point of approach (CPA) to the VLA. The location where $\beta = \infty$ occurs at the CPA. The curvature of the striation pattern in the time-frequency plane is dependent on both the ship speed and CPA distance. A 20-min time interval was used to best visualize the hyperbola pattern for ships with ship speed and CPA distances seen in this study. The ship noise spectrograms are useful due to the tendency of merchant ships to travel in straight paths at constant speed (i.e., uniform motion) and the availability of information regarding the geographical coordinates of ships, which are publicly available via the MarineTraffic Automatic Identification System (AIS) database.²⁶

During its deployment, 184 ships passed within 15 km of PROTEUS. However, not all ships are clearly visible on the spectrograms of the processed data. Some ships were too

far away or too quiet to produce an adequate signal-to-noise ratio (SNR) to determine the frequencies at which $\beta = \infty$. For this analysis, 24 ships of interest were chosen with ship tracks that fall into three categories: northern lane, southern lane, and “other.” The average distances from ships in the southern lane to the three arrays VLA1, PROTEUS, and VLA2 are 5.9, 4.9, and 2.6 km, respectively. The average distances from the northern lane ships are 8.3, 9.6, and 11.4 km, listed in the same order. A map of the geographical area, shipping lanes, locations of the line arrays, and plots of the ship tracks is shown in Fig. 2. Of the 24 ships, only 3 ships deviated from the northern and southern shipping lanes and fell into the “other” track category. Some ships traveled through the area repeatedly during the deployment of the arrays. For the ships with multiple travel paths through the area, only those having an adequate SNR were included in this analysis.

The 24 ship spectrograms from SBCEX 2022 were analyzed to find the frequencies at which $\beta = \infty$. In the NEMP, these singular points occur in the 20–80 Hz band. A careful analysis of the singular points for each of the 24 ships of interest showed as many as three points for some ships. These singular points were associated with $\beta_{1,2}$, $\beta_{1,3}$, and $\beta_{1,4}$, and the corresponding frequencies were defined as $f_{1,2}$, $f_{1,3}$, and $f_{1,4}$. Though β is independent of receiver depth, an examination of the spectrograms from every channel of the VLAs was necessary to observe all singular points. This level of analysis was required because at certain depths, some modes have nulls in the depth-dependent mode function and the singular point related to that mode was not evident.

The $f_{1,2}$ values for each ship are shown in Fig. 3. The ships are ordered by their track category, sequentially with the southern track first, then the northern track, and finally

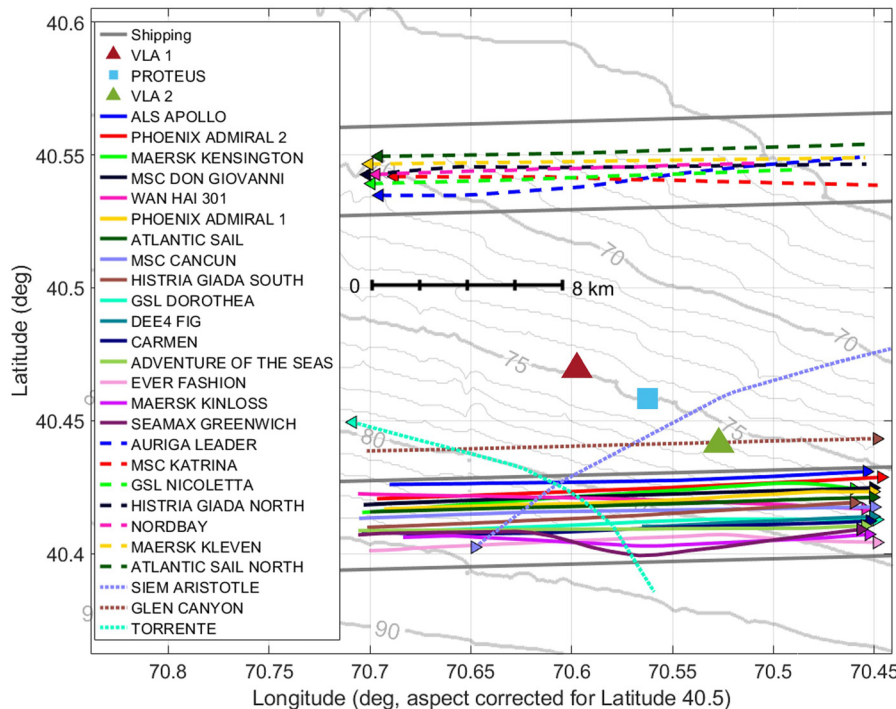


FIG. 2. (Color online) Map of the paths of 24 ships that passed through the area during SBCEX 2022. The gray lines indicate the depth contour lines.

29 October 2024 21:46:19

the “other” track. Clear clusters separating the $f_{1,2}$ values of ships appear in Fig. 3, differentiating the southern tracks from the northern tracks. Additionally, in the southern shipping lane, three groupings of $f_{1,2}$ values exist corresponding to the three arrays. MSC *Cancun*, a container ship with a southern lane track, was detected by all three arrays; the $f_{1,2}$ values shift gradually between arrays, as shown in Fig. 4. The ships with “other” tracks also have their own cluster in Fig. 3, even though their tracks were all unique from each other.

The singular frequencies are sensitive to everything in the environment. However, the 2017 waveguide invariant study used pre-modeling to show that the singular frequencies are more sensitive to the characteristics of the deeper layers of the seabed.¹³ Additionally, a comparison of the $f_{1,2}$ values for ships on the southern track between 2017 and 2022 shows that the shift between years is minimal, despite the variation in the water column sound speeds as shown in Fig. 1.

To quantify the closeness of the average $f_{1,2}$ values detected by VLA1 and VLA2 from 2017 to the different array groupings found in 2022, we calculated the centroids of the three array groupings for the three southern lane ships (*Carmen*, MSC *Cancun*, and ALS *Apollo*), as shown in Fig. 3. The centroids were then compared to the average $f_{1,2}$ values for southern ships from 2017 as detected by VLA1 and VLA2 from Ref. 13. For ships detected by VLA1 in 2017, the distances between the average $f_{1,2}$ value and the centroid of the 2022 groupings were +0.9 Hz for VLA1, -0.7 Hz for PROTEUS, and -1.4 Hz for VLA2. For VLA2, the distances between the average value for 2017 and the centroid for the three arrays from 2022 were +2.1 Hz for VLA1, +0.5 Hz for PROTEUS, and -0.2 Hz for VLA2.

These differences reveal consistency between the 2017 and 2022 singular frequencies. For VLA2, the average of $f_{1,2}$ from 2017 is most closely clustered with the values from

the same array location in 2022. For VLA1, the average of $f_{1,2}$ falls between the clusters found for data recorded from PROTEUS and VLA1. Due to lack of significant differences in the $f_{1,2}$ values between 2017 and 2022 for a single VLA, differences in the singular frequencies for ships with different tracks, as seen in this study, point towards heterogeneity in the deep sediment layers, rather than differences in the water column. Furthermore, these differences may reveal heterogeneity from north to south in the NEMP as well as east to west in the southern shipping lane.

D. Inference method

The frequencies associated with the singular points are used as the input for a maximum entropy feature-based inversion to infer estimates of the deep seabed characteristics. For each ship noise spectrogram, the $f_{1,2}$, $f_{1,3}$, and $f_{1,4}$ values were extracted and compared to the modeled frequency values $\hat{f}_{m,n}$, labeled as $\hat{f}_{1,2}$, $\hat{f}_{1,3}$, and $\hat{f}_{1,4}$. The $\hat{f}_{m,n}$ values are obtained by identifying the frequencies at which the group velocity for modes $m = 1$ and $n = 2, 3, 4$, found using ORCA (Ref. 27) and the ocean environment θ , are equal. The data-model mismatch is quantified via the cost function:

$$E(\theta) = \frac{1}{2} \sum_{n=2}^4 (f_{1,n} - \hat{f}_{1,n}(\theta))^2. \tag{3}$$

The ocean environment is specified by the seabed and water column. For the inversion, most of the seabed parameters are held constant, as shown in Table II. Estimates for the properties of the top three sediment layers come from Belcourt *et al.*,²⁸ where a viscous grain shearing (VGS) model was used to infer the depth dependence of the geoaoustic properties with a transdimensional Bayesian approach. The thickness of the mud throughout the NEMP

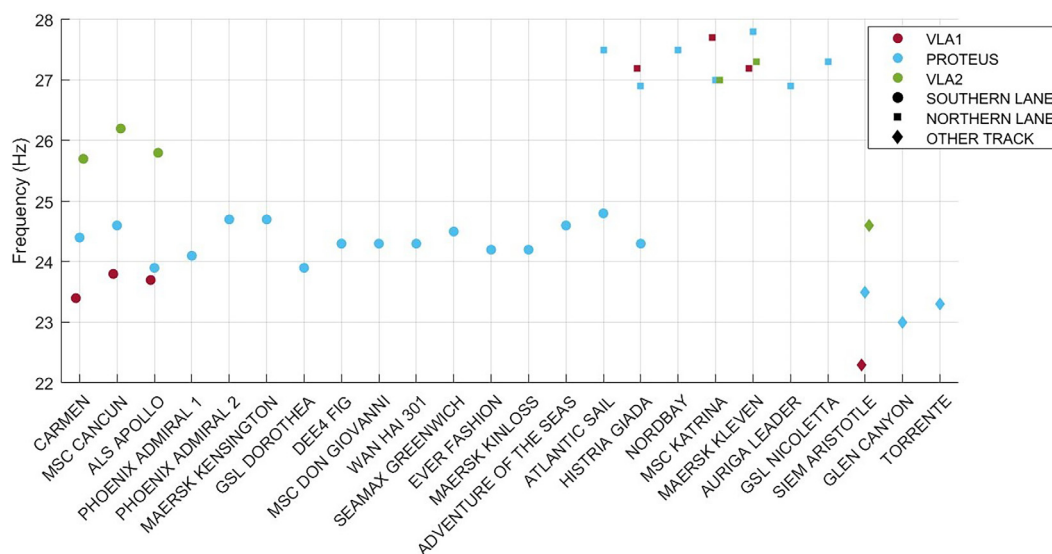


FIG. 3. (Color online) The $\beta_{1,2}$ frequencies for 24 ships of interest. Ships with southern ship tracks are listed first, followed by northern and “other” tracks.

is variable; however, the values utilized for the top three layers match the sediment properties in the thickest part of the NEMP, where all three VLAs were located. Their findings of a transition layer between the mud and sand are consistent with both core samples from Twichell *et al.*⁴ and results from the sub-bottom layering measurements.⁵ The properties of these first three layers (mud, transition, and sand) were held fixed, as well as the properties of a final deep layer, deep layer 3 (DL3), and the basement. As the

water column varied throughout the experiment and geographical area, as shown in Fig. 1, the sound speed profile that was closest in time and location to each ship was used in the inversion.

The thickness and sound speeds of deep layers 1 and 2 (DL1 and DL2, respectively) were sampled for 4000 Monte Carlo iterations. The numbers in brackets from Table II for these parameters indicate the upper and lower bounds. For each ship, the set of DL1 and DL2 sound speeds and thicknesses that returned the lowest cost function between the frequencies of the modeled and measured singular points are identified as the best-fit parameters.

The best-fit parameters are used to obtain modeled spectrograms for each of the ships. To compare the measured received levels and the modeled levels, the source spectral level must be accounted for. Previous studies have indicated that the Wales–Heitmeyer source spectrum²⁹ does not adequately reflect VLF noise from merchant ship noise. Instead, an estimate of the source level, for each ship, is obtained by adding the transmission loss modeled with ORCA using the best-fit parameters (TL_{opt}) to the measured power spectral density levels (PSD_{meas}) and finding the mean values over time. Specifically, the estimated source level at frequency f_j ,

$$SL(f_j) = \frac{1}{N_t} \sum_{i=1}^{N_t} [PSD_{meas}(f_j) + TL_{opt}(f_j)], \quad (4)$$

where N_t is the number of time steps in the spectrogram. The modeled spectrograms are plotted as $PSD_{model} = SL - TL_{opt}$.

The Monte Carlo sampling and lowest cost function values are utilized in maximum entropy to estimate the marginal probability distributions of the four inferred parameters. The likelihood function for the parameters is calculated for the m th iteration,

$$p_m(\theta) \propto \frac{1}{Z} \exp \left\{ -\frac{1}{T} E_m(\theta) \right\}, \quad (5)$$

where E is the error from Eq. (3). The normalization factor (Z) is

$$Z = \sum_{m=1}^M \exp \left\{ -\frac{E_m(\theta)}{T} \right\}, \quad (6)$$

where M is the total number of Monte Carlo iterations. The maximum entropy “temperature” T (calculated with the lowest cost function value for each ship) is

$$T \approx \frac{2}{N} \min E_m(\theta), \quad (7)$$

where N is the number of parameters used in the statistical inverse problem. The justification for using Eq. (7) comes from an analogy with the equipartition theorem in thermodynamics.^{30,31}

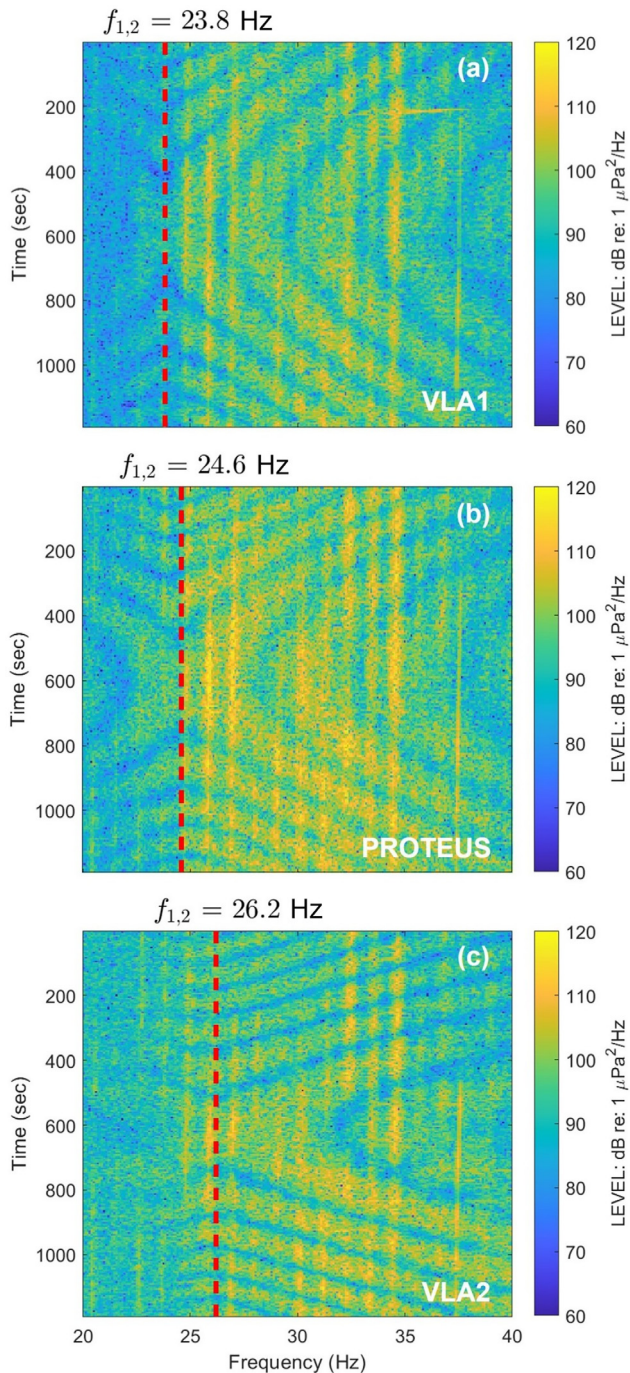


FIG. 4. (Color online) The measured data for MSC Cancun (southern shipping lane). The ship was detected by all three arrays: (a) VLA1 at a depth of 41 m, (b) PROTEUS at a depth of 45 m, and (c) VLA2 at a depth of 15 m.

TABLE II. Prior model of seabed.^a

Layer	Thickness(m)	Sound speed (m/s)		Density (kg/m ³)	Attenuation (dB at 1 kHz)
		Top	Bottom		
Mud	9.2	1445	1446	1.62	0.04
Transition	3.0	1446	1750	1.80	0.15
Sand	7.5	1750	1750	1.83	0.15
DL1	[50, 300]	[1700, 1810]	DL1_SS _{top}	2.00	0.15
DL2	[50, 300]	[1815, 2050]	DL2_SS _{top}	2.20	0.15
DL3	100.0	2100	2100	2.20	0.15
Basement		2350	2350	2.60	0.22

^aFor DL1 and DL2, the numbers in brackets correspond to the values of the upper and lower bounds used in the Monte Carlo sampling. SS, sound speed.

III. RESULTS

The maximum entropy inversion of the 24 ships of interest resulted in estimates of the DL1 and DL2 sound speeds. Examples of the inference process are provided along with the estimates obtained using all 24 ships. Similar to the clusters observed in the $\beta_{1,2}$ frequencies of the 24 ships in Fig. 3, the sound speeds of DL1 in the NEMP also showed clusters based on location. These estimates are effective properties over the propagation path and, in this work, are associated with the coordinates of ships at their CPA to the VLAs. Plots of the estimated sound speeds

versus geographical coordinate of each ship at CPA show heterogeneity of the deep layer.

A. Example of the inference process

Container ship *MSC Don Giovanni* traveled through the southern shipping lane, with a CPA range of 4.12 km from the PROTEUS array. The measured spectrograms for *MSC Don Giovanni* are shown in Fig. 5. Two different channels were used to extract the $f_{1,2}$ and $f_{1,3}$ values from the measured data. In Fig. 5(a), the spectrogram from channel 17 (depth = 8.5 m) shows a clear “x” at the $\beta_{1,2} = \infty$ point at 24.3 Hz. In contrast, as shown in Fig. 5(b), the spectrogram from channel 11 (depth = 26.5 m) exhibits the same pattern for both $\beta_{1,2}$ and also $\beta_{1,3}$ at 38.0 Hz.

Using the singular frequencies, a feature-based inversion was performed. The resulting modeled spectrogram with the optimal seabed parameters from the statistical inference are shown in Fig. 6. Though the $\hat{f}_{1,2}$ and $\hat{f}_{1,3}$ values of 23.8 and 38.5 Hz, respectively, from the modeled spectrogram do not exactly match the $f_{1,2}$ and $f_{1,3}$ values (Fig. 5), they are similar, with a mean squared error of 0.284 Hz².

The modeled modal group velocities can be examined to determine the m and n values associated with the singular frequencies. A plot of the group velocities of the first four

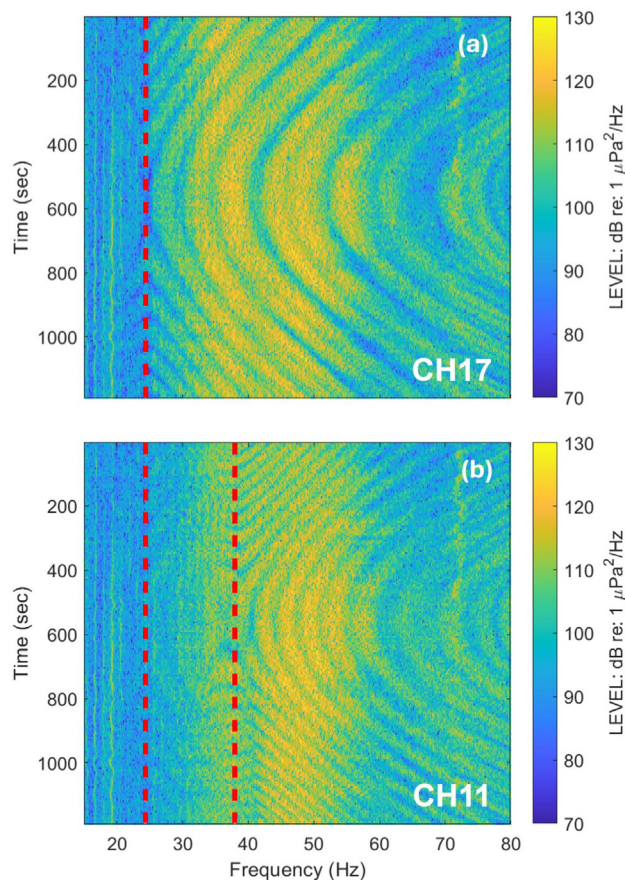


FIG. 5. (Color online) The measured spectrograms of *MSC Don Giovanni* collected by PROTEUS by two different channels, where (a) shows $f_{1,2} = 24.3$ Hz on channel 17 and (b) shows $f_{1,2}$ and $f_{1,3} = 38.0$ Hz on channel 11.

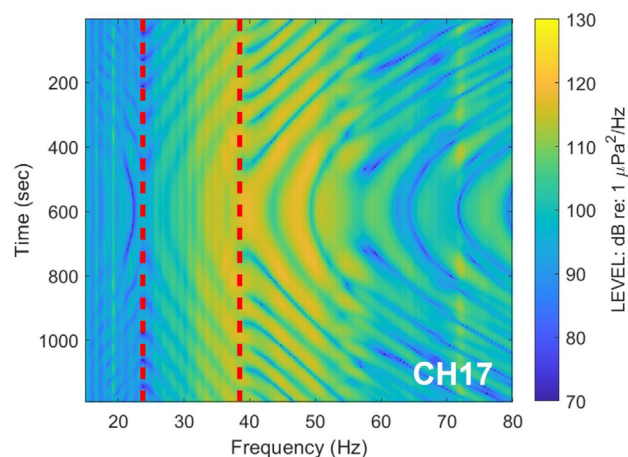


FIG. 6. (Color online) The modeled spectrogram using the deep layer properties obtained from the maximum entropy inversion from the *MSC Don Giovanni* has $\hat{f}_{1,2} = 23.8$ Hz and $\hat{f}_{1,3} = 38.5$ Hz.

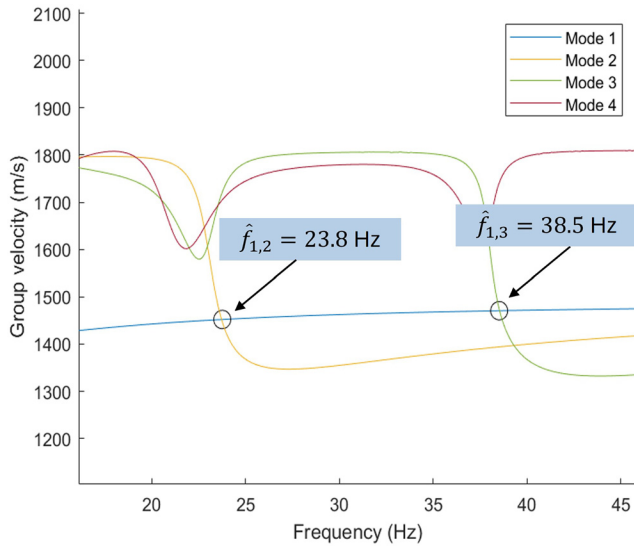


FIG. 7. (Color online) The modal group velocities using the optimal seabed parameters for MSC *Don Giovanni*.

modes using the optimal seabed parameters with ORCA is shown in Fig. 7 and confirm that the frequencies where modes 1 and 2 and modes 1 and 3 cross approximately match the singular frequencies in the modeled spectrogram (Fig. 7).

The maximum entropy inversion yields posterior probability distributions for the four inferred parameters. The marginal probability distributions for the four parameter values are shown in Fig. 8. The only parameter with an informative distribution is the sound speed of DL1. In this case, the optimal sound speed of 1815 m/s (which yields the lowest cost) and the sound speed from the peak of the marginal probability distribution of 1814 m/s are in good agreement.

An informative distribution for DL1 sound speed was obtained for all ships, with only a few ships having informative distributions for other parameters. The probability distributions using data from the noise generated by MSC *Don Giovanni*, specifically, also suggest a limiting value of the thickness of DL1. Though the distribution does not have a peaked value, one can infer that the thickness is greater than 175 m based on the asymmetrical shape of the distribution.

The maximum entropy inference analysis, as described for the ship MSC *Don Giovanni*, was done for all 24 ships of interest. For each ship, the maximum entropy inversion yielded values for deep layer properties that minimized the cost between the $f_{m,n}$ and $\hat{f}_{m,n}$. A comparison of the measured and modeled spectrograms for three ships from the three different track categories is shown in Fig. 9. The dashed line indicates the singular points with the labeled $f_{1,2}$ or $\hat{f}_{1,2}$ values. The deep layer properties were grouped into their track category and compared to the seabed parameter estimates from other travel categories. This was done to determine the extent of the spatial variability of DL1 and DL2.

B. Seabed heterogeneity

An analysis of DL1 sound speeds corroborates the initial hypothesis of heterogeneity in the seabed. The sound speed values associated with the peak in the marginal probability distributions for all ships are shown in Fig. 10, with error bars that indicate the standard deviation of the marginal probability distributions. The ships are ordered from the closest CPA to PROTEUS to farthest. Once again, a statistically distinguishable separation is apparent between the sound speeds inferred from ships with southern lane tracks

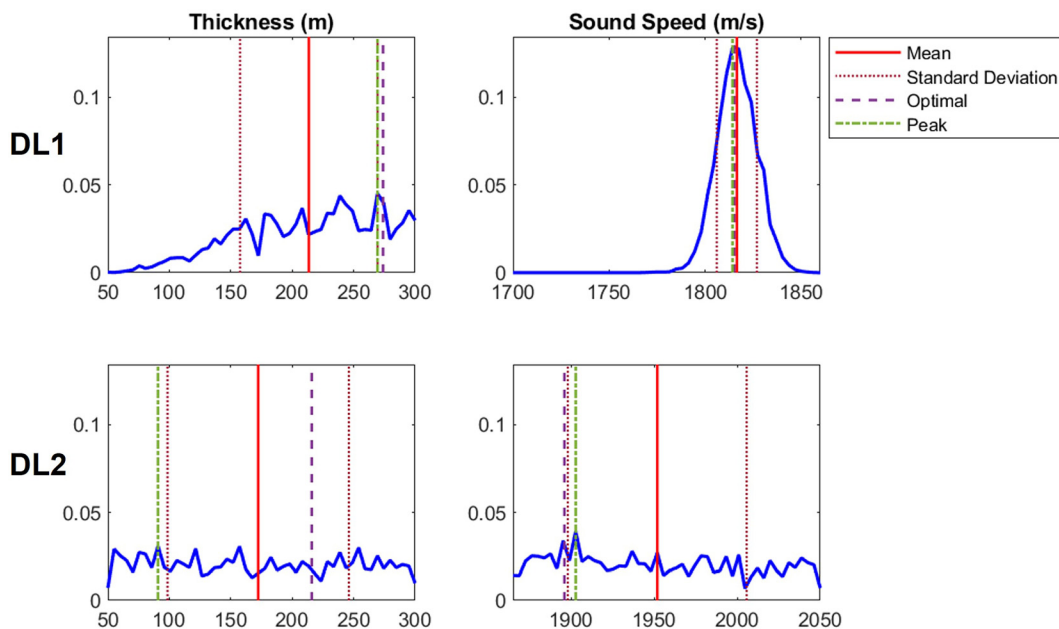


FIG. 8. (Color online) The marginal probability distributions for four deep layer parameters using the maximum entropy inversion on MSC *Don Giovanni*. The optimal values (purple dashed lines) are associated with the lowest cost function and are used to produce the modeled spectrograms.

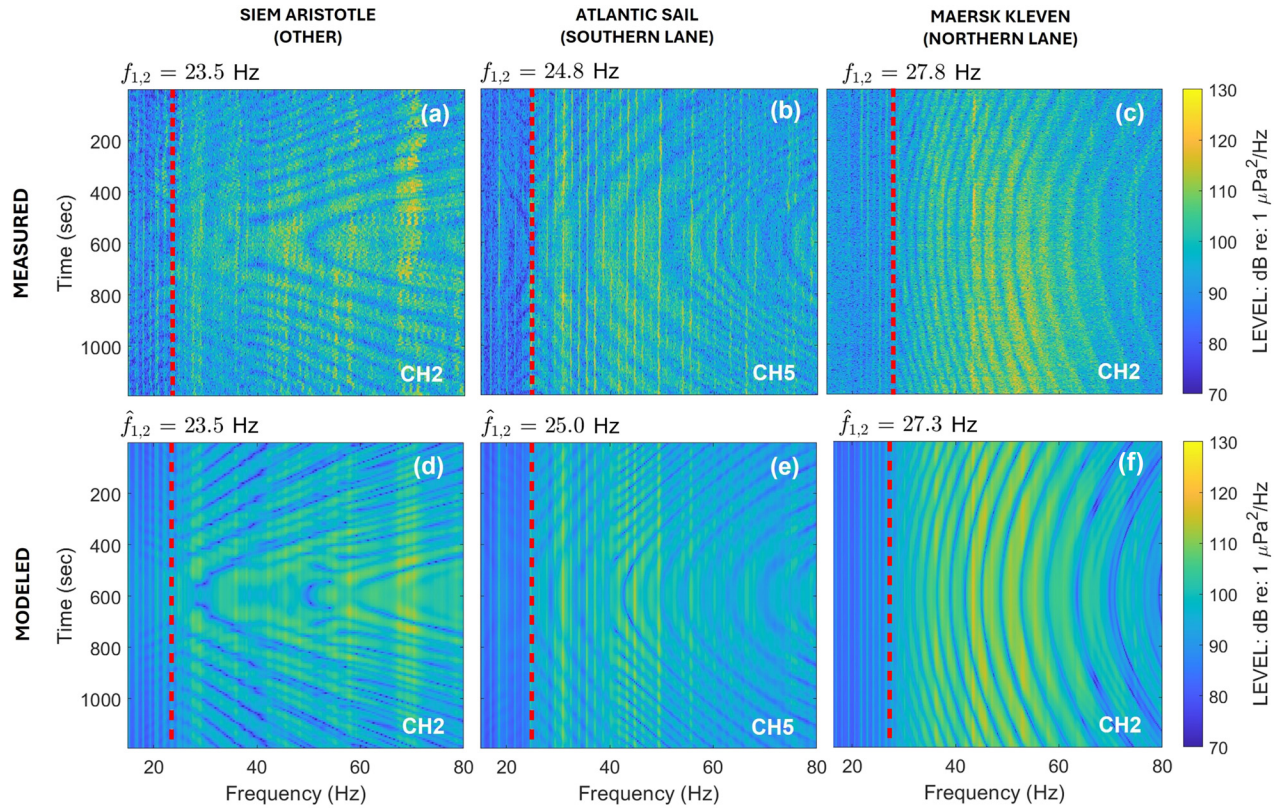


FIG. 9. (Color online) (a–c) The measured spectrograms for three different ships collected by PROTEUS. (d–f) The modeled spectrograms using the optimal deep layer parameter values after the inversion was performed. The red dashed line shows the $\beta = \infty$ singular points.

and those with northern lane tracks. The range of estimated sound speeds for DL1 is 1710–1820 m/s.

As mentioned previously, the seabed parameters for the top three layers of the ocean environment were held fixed, at values associated with the location of the VLAs in the thickest part of the mud, for the maximum entropy process. Specifically, the mud thickness was fixed at 9.2 m and the water depth held at a fixed depth of 75 m. This approach is an approximation because the water depth varied from 65 to

70 m in the northern shipping lane and 77 to 84 m in the southern shipping lane. Additionally, the mud thickness varied across the sound propagation path from thicknesses of about 3 m in the northern shipping lane and to thicknesses of 4.5–7 m in the southern shipping lane. (These mud thicknesses were estimated from Fig. 2 in Wilson *et al.*¹¹)

Due to the heterogeneity of the top layers of the ocean sediment, a more complete study of the deep layers would require a range-dependent propagation model. As an

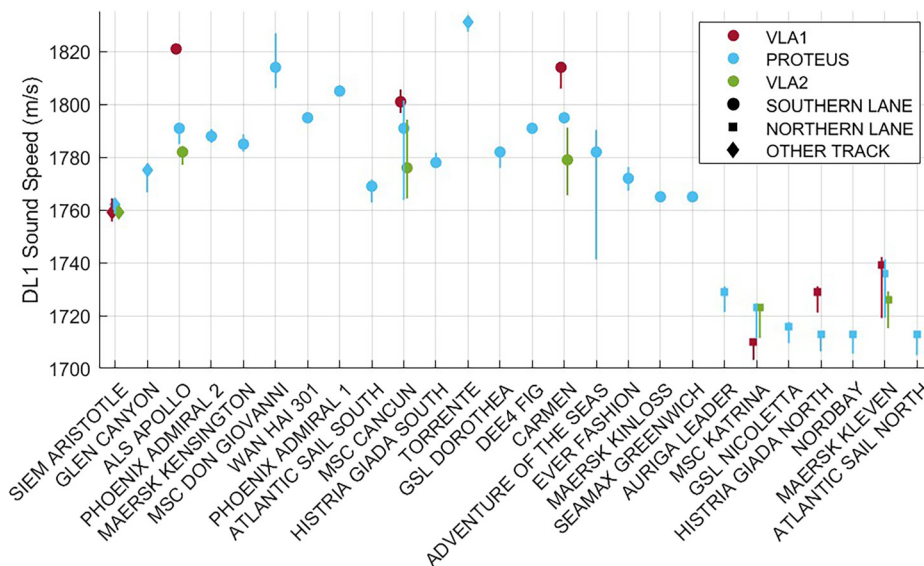


FIG. 10. (Color online) The DL1 peak sound speeds for all ships of interest based on the marginal probability distribution. The bars indicate the standard deviation of the sound speeds derived from the marginal probability distribution.

approximation to bound the DL1 sound speed estimates, the maximum entropy analysis was applied twice on several select ships. First, estimates were made for the DL1 sound speed by using a water depth and mud thickness matching the receiver (VLA) environment, and then a second set of estimates was obtained using the water depth and mud thickness at the average acoustical source locations (i.e., ship CPA locations). A plot of the inferred DL1 sound speeds associated with fixed seabeds from both the source and receiver locations of the five ships selected is shown in Fig. 11. A definitive shift in the sound speeds between the receiver environment and source environment is evident for all five cases. The direction of the shift is the same for all but one case. By bounding the problem in this way, one still observes that the DL1 sound speeds from southern lane ships are grouped at higher sound speeds than the northern lane ships. This supports the claim of deep layer heterogeneity in the NEMP.

A plot of the sound speed on a map of the NEMP, as shown in Fig. 12, provides further insight into the nature of the heterogeneity of the deep layers. The DL1 sound speeds are the values obtained with the original maximum entropy inversion where a mud thickness of 9.2 m was assumed (Fig. 10). For a homogeneous horizontally stratified environment, one would expect the sound speed of the deep layer to be the same throughout the geographical area; however, this is not the case. Not only are the sediment sound speeds between the northern and southern areas of the NEMP distinguishable, but a gradual change is also observed in the sound speeds going from east to west in the southern shipping lane. Furthermore, the points above the southern

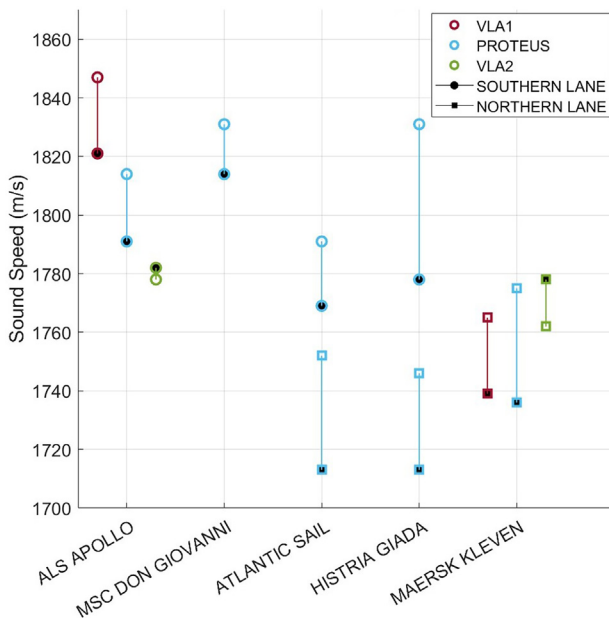


FIG. 11. (Color online) A comparison of the inferred DL1 sound speeds using the model ocean environment for the water depth and mud thickness at both the source and receiver locations. The solid points were inferred using the receiver environment and the open points with the source ocean environment.

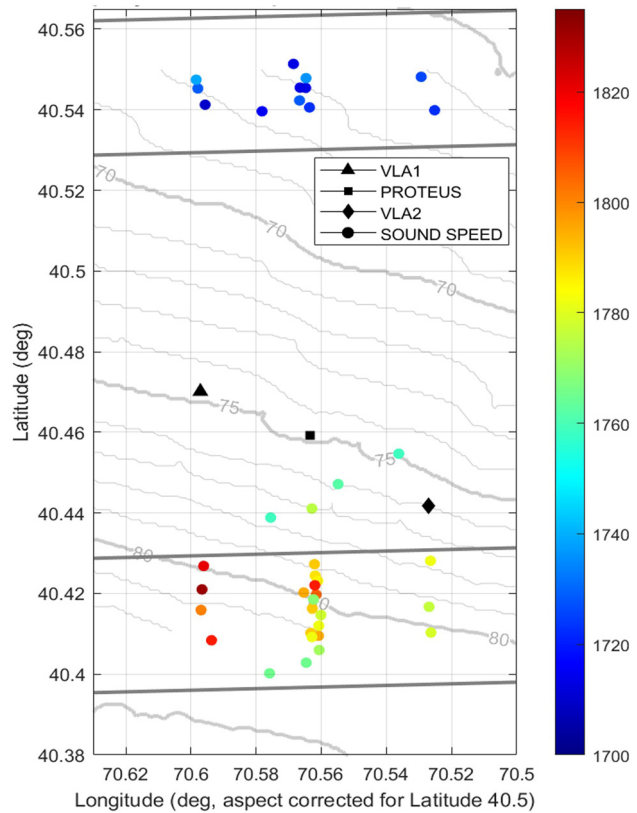


FIG. 12. (Color online) The sound speed of DL1 at discrete latitude and longitude coordinates.

shipping lane closest to the arrays show sound speeds in between those found in the northern and southern parts, suggesting a gradual spatial shift in the sound speeds of DL1.

IV. CONCLUSIONS

Singular points where the waveguide invariant goes to infinity ($\beta_{m,n} \rightarrow \infty$) were observed in VLF spectrograms of merchant ships in the NEMP for data collected during SBCEX 2022. The singular points are associated with frequencies where pairs of modes have equal group velocities. These singular frequencies associated with 24 ships traveling in either the northern or southern shipping lanes or deviating from the lanes (“other” tracks) showed clusters that were statistically distinct. The signals were captured on three line arrays placed between shipping lanes, which also showed gradual shifts in the singular points along the southern shipping lane. The singular frequencies were used as features in a statistical inference methodology to estimate deep layer parameters of the seabed. A prior model was used where the top three layers of mud, the transition, and the sand were assumed fixed, as in the 2017 waveguide invariant study.¹⁴

Results from the maximum entropy inversion indicated that the only informative marginal probability distribution obtained from the singular points was for the sound speed of the first deep layer. The sound speeds of the deep layer ranged between 1710 m/s and 1820 m/s. Sound speeds from

the northern shipping lane were lower than those in the southern shipping lane, and there was a gradual shift in the sound speeds from east to west in the southern shipping lane. Because the estimates obtained using sound propagation from the southern and northern tracks are statistically distinguishable, there is enough resolution to infer heterogeneity in the seabed. These results have possible implications for future work using merchant ship noise as a tool to estimate spatial variability of deep sediment layers that would traditionally require extensive geological surveys and/or large-scale seismic studies.

ACKNOWLEDGMENTS

This study was supported by the Office of Naval Research, Contract/Grant Nos. N00014-22-P-2007, N00014-22-1-2128, N00014-20-1-2781, and N00014-21-1-2789. D.P.K. wishes to acknowledge Dr. Robert A. Koch for many helpful discussions on the use of low frequency ship noise in geoacoustic inversion studies.

AUTHOR DECLARATIONS

Conflict of Interest

The authors have no conflicts to disclose.

DATA AVAILABILITY

The data that support the findings of this study are available from the corresponding author upon reasonable request. The MPL data are available from W.S.H., MPL. The ARL data are available from P.S.W. and J.D.S., ARL.

¹G. R. Potty, J. H. Miller, and J. F. Lynch, "Inversion for sediment geoacoustic properties at the New England Bight," *J. Acoust. Soc. Am.* **114**(4), 1874–1887 (2003).
²J. H. Miller, L. R. Bartek, G. R. Potty, D. Tang, J. Na, and Y. Qi, "Sediments in the East China Sea," *IEEE J. Ocean. Eng.* **29**(4), 940–951 (2004).
³J. Bonnel and N. R. Chapman, "Geoacoustic inversion in a dispersive waveguide using warping operators," *J. Acoust. Soc. Am.* **130**(2), EL101–EL107 (2011).
⁴D. C. Twichell, C. E. McClennen, and B. Butman, "Morphology and processes associated with the accumulation of the fine-grained sediment deposit on the southern New England shelf," *J. Sedimentary Res.* **51**(1), 269–280 (1981).
⁵J. A. Goff, A. H. Reed, G. Gawarkiewicz, P. S. Wilson, and D. P. Knobles, "Stratigraphic analysis of a sediment pond within the New England Mud Patch: New constraints from high-resolution chirp acoustic reflection data," *Mar. Geol.* **412**, 81–94 (2019).
⁶J. A. Goff, D. J. Swift, C. S. Duncan, L. A. Mayer, and J. Hughes-Clarke, "High-resolution swath sonar investigation of sand ridge, dune and ribbon morphology in the offshore environment of the New Jersey margin," *Mar. Geol.* **161**(2–4), 307–337 (1999).
⁷J. Goff, H. Olson, and C. Duncan, "Correlation of side-scan backscatter intensity with grain-size distribution of shelf sediments, New Jersey margin," *Geo-Mar. Lett.* **20**(1), 43–49 (2000).
⁸C. S. Duncan, J. A. Goff, J. A. Austin, Jr., and C. S. Fulthorpe, "Tracking the last sea-level cycle: Seafloor morphology and shallow stratigraphy of the latest Quaternary New Jersey middle continental shelf," *Mar. Geol.* **170**(3–4), 395–421 (2000).
⁹E. L. Hamilton, "Sound velocity gradients in marine sediments," *J. Acoust. Soc. Am.* **65**(4), 909–922 (1979).

¹⁰E. L. Hamilton, "Geoacoustic modeling of the sea floor," *J. Acoust. Soc. Am.* **68**(5), 1313–1340 (1980).
¹¹P. S. Wilson, D. P. Knobles, and T. B. Neilsen, "Guest editorial an overview of the Seabed Characterization Experiment," *IEEE J. Ocean. Eng.* **45**(1), 1–13 (2020).
¹²J. Siegel, B. Dugan, D. Lizarralde, M. Person, W. DeFoor, and N. Miller, "Geophysical evidence of a late Pleistocene glaciation and paleo-ice stream on the Atlantic Continental Shelf offshore Massachusetts, USA," *Mar. Geol.* **303–306**, 63–74 (2012).
¹³D. Knobles, P. S. Wilson, T. B. Neilsen, and W. S. Hodgkiss, "Influence of seabed on very low frequency sound recorded during passage of merchant ships on the New England shelf," *J. Acoust. Soc. Am.* **149**(5), 3294–3300 (2021).
¹⁴D. Knobles, T. Neilsen, P. Wilson, W. Hodgkiss, J. Bonnel, and Y. Lin, "Maximum entropy inference of seabed properties using waveguide invariant features from surface ships," *J. Acoust. Soc. Am.* **151**(5), 2885–2896 (2022).
¹⁵W. G. Zhang and G. G. Gawarkiewicz, "Dynamics of the direct intrusion of Gulf Stream ring water onto the mid-Atlantic Bight shelf," *Geophys. Res. Lett.* **42**(18), 7687–7695, <https://doi.org/10.1002/2015GL065530> (2015).
¹⁶T. F. Duda, W. G. Zhang, K. R. Helfrich, A. E. Newhall, Y.-T. Lin, J. F. Lynch, P. F. Lermusiaux, P. Haley, and J. Wilkin, "Issues and progress in the prediction of ocean submesoscale features and internal waves," in *2014 Oceans-St. John's*, St. John's, Newfoundland, Canada (IEEE, New York, 2014), pp. 1–9.
¹⁷G. L. D'Spain and W. A. Kuperman, "Application of waveguide invariants to analysis of spectrograms from shallow water environments that vary in range and azimuth," *J. Acoust. Soc. Am.* **106**(5), 2454–2468 (1999).
¹⁸S. D. Chuprov, "Interference structure of a sound field in a layered ocean," in *Ocean Acoustics, Current Status*, edited by L. M. Brekhovskikh and I. B. Andreyeva (Nauka, Moscow, 1982), pp. 71–91.
¹⁹A. Turgut, M. Orr, and D. Rouseff, "Broadband source localization using horizontal-beam acoustic intensity striations," *J. Acoust. Soc. Am.* **127**(1), 73–83 (2010).
²⁰K. D. Heaney, "Rapid geoacoustic characterization using a surface ship of opportunity," *IEEE J. Ocean. Eng.* **29**(1), 88–99 (2004).
²¹Q.-y. Ren and J.-P. Hermand, "Acoustic interferometry for geoacoustic characterization in a soft-layered sediment environment," *J. Acoust. Soc. Am.* **133**(1), 82–93 (2013).
²²C. Verlinden, J. Sarkar, B. D. Cornuelle, and W. A. Kuperman, "Determination of acoustic waveguide invariant using ships as sources of opportunity in a shallow water marine environment," *J. Acoust. Soc. Am.* **141**(2), EL102–EL107 (2017).
²³Y. Le Gall and J. Bonnel, "Passive estimation of the waveguide invariant per pair of modes," *J. Acoust. Soc. Am.* **134**(2), EL230–EL236 (2013).
²⁴S. Piao, Y. Dong, Z. Wu, X. Wang, and G. Zheng, "Geoacoustic inversion using very-low-frequency modal interference characteristics," *JASA Express Lett.* **3**(6), 066004 (2023).
²⁵R. A. Koch and D. P. Knobles, "Geo-acoustic inversion from surface ships," *J. Acoust. Soc. Am.* **117**(1), 626–637 (2005).
²⁶Bureau of Ocean Energy Management (BOEM) and National Oceanic and Atmospheric Administration (NOAA), "MarineCadastre.gov. [Area of Interest: Top left = 40.8, -71.3; bottom right = 39.7, -70.1]. [Dates: 07-May-22 to 3-Jun-22]," <https://marinecadastre.gov/ais/> (Last viewed June 10, 2023).
²⁷E. K. Westwood, C. T. Tindle, and N. R. Chapman, "A normal mode model for acousto-elastic ocean environments," *J. Acoust. Soc. Am.* **100**(6), 3631–3645 (1996).
²⁸J. Belcourt, C. W. Holland, S. E. Dosso, J. Dettmer, and J. A. Goff, "Depth-dependent geoacoustic inferences with dispersion at the New England Mud Patch via reflection coefficient inversion," *IEEE J. Ocean. Eng.* **45**(1), 69–91 (2020).
²⁹S. C. Wales and R. M. Heitmeyer, "An ensemble source spectra model for merchant ship-radiated noise," *J. Acoust. Soc. Am.* **111**(3), 1211–1231 (2002).
³⁰J. R. Nuttal, T. B. Neilsen, and M. K. Transtrum, "Maximum entropy temperature selection via the equipartition theorem," *Proc. Mtgs. Acoust.* **52**(1), 070004 (2023).
³¹F. Reif, *Statistical and Thermal Physics* (McGraw-Hill, New York, 1965).